ORIGINAL ARTICLE

Microbial metabolite deoxycholic acid promotes vasculogenic mimicry formation in intestinal carcinogenesis

Xueli Song[1] | Yaping An[1] | Danfeng Chen[1] | Wanru Zhang[1] | Xuemei Wu[1] |
Chuqiao Li[1] | Sinan Wang[1] | Wenxiao Dong[1] | Bangmao Wang[1] | Tianyu Liu[1] |
Weilong Zhong[1] | Tao Sun[2] | Hailong Cao[1] 🄳

[1]Department of Gastroenterology and Hepatology, General Hospital, Tianjin Institute of Digestive Diseases, Tianjin Key Laboratory of Digestive Diseases, Tianjin Medical University, Tianjin, China

[2]State Key Laboratory of Medicinal Chemical Biology and College of Pharmacy, Nankai University, Tianjin, China

Correspondence
Hailong Cao and Weilong Zhong, Department of Gastroenterology and Hepatology, General Hospital, Tianjin Medical University, Tianjin 300052, China.
Email: caohailong@tmu.edu.cn; zhongweilong@tmu.edu.cn

Tao Sun, State Key Laboratory of Medicinal Chemical Biology and College of Pharmacy, Nankai University, Tianjin 300350, China.
Email: sunrockmia@hotmail.com

Funding information
National Natural Science Foundation of China, Grant/Award Number: 81970477 and 82070545; the Key Project of Science and Technology Pillar Program of Tianjin, Grant/Award Number: 20YFZCSY00020

Abstract

A high-fat diet (HFD) leads to long-term exposure to gut microbial metabolite secondary bile acids, such as deoxycholic acid (DCA), in the intestine, which is closely linked to colorectal cancer (CRC). Evidence reveals that vasculogenic mimicry (VM) is a critical event for the malignant transformation of cancer. Therefore, this study investigated the crucial roles of DCA in the regulation of VM and the progression of intestinal carcinogenesis. The effects of an HFD on VM formation and epithelial-mesenchymal transition (EMT) in human CRC tissues were investigated. The fecal DCA level was detected in HFD-treated $Apc^{min/+}$ mice. Then the effects of DCA on VM formation, EMT, and vascular endothelial growth factor receptor 2 (VEGFR2) signaling were evaluated in vitro and in vivo. Here we demonstrated that compared with a normal diet, an HFD exacerbated VM formation and EMT in CRC patients. An HFD could alter the composition of the gut microbiota and significantly increase the fecal DCA level in $Apc^{min/+}$ mice. More importantly, DCA promoted tumor cell proliferation, induced EMT, increased VM formation, and activated VEGFR2, which led to intestinal carcinogenesis. In addition, DCA enhanced the proliferation and migration of HCT-116 cells, and induced EMT process and vitro tube formation. Furthermore, the silence of VEGFR2 reduced DCA-induced EMT, VM formation, and migration. Collectively, our results indicated that microbial metabolite DCA promoted VM formation and EMT through VEGFR2 activation, which further exacerbated intestinal carcinogenesis.

KEYWORDS
colorectal cancer, deoxycholic acid, epithelial-mesenchymal transition, vascular endothelial growth factor receptor 2, vasculogenic mimicry

---

---

1 | INTRODUCTION

Colorectal cancer (CRC) is characterized by high morbidity and mortality rates.[1] The risk factors for the progression of CRC include age, sex, a high-fat diet (HFD), obesity, diabetes, race/ethnicity, smoking, and gene mutation. The prevention and treatment of CRC remain a challenge.[2-4] An HFD results in increased secretion and excretion of hepatic primary bile acids (BAs), which are further metabolized by gut microbiota into secondary BAs, such as deoxycholic acid (DCA).[5,6] As a microbial metabolite, it has been suggested that DCA is an important pro–tumor factor correlated with increased colon cancer risk.[7] A meta-analysis showed that there were no significant differences in DCA, lithocholic acid (LCA) and primary and secondary BAs between CRC patients and controls.[8] However, a recent prospective study showed that pre–diagnostic levels of certain conjugated primary and secondary BAs were positively associated with the risk of colon cancer.[9] Hence, it is necessary to further study the relationship between and mechanisms of microbial metabolite DCA and CRC. Previous studies have shown that DCA could promote CRC progression through multiple mechanisms, such as intestinal barrier disruption, chronic inflammation, and gut dysbiosis.[10-12] However, the role of DCA in the blood supply in intestinal carcinogenesis remains to be further elucidated.

Distinct from classical tumor angiogenesis, vasculogenic mimicry (VM), independent of endothelial vessels, is the fluid-conducting channel system lining with tumor cells and containing red blood cells.[13,14] The VM simulates endothelial vascular function to deliver oxygen and nutrients and eliminate waste to rapidly promote tumor proliferation.[15,16] VM was first elaborated as a form of new 65vessels in highly aggressive uveal melanoma by Maniotis et al in 1999.[17] The various molecular mechanisms are closely related to the VM formation of tumors, mainly involving vascular endothelial growth factor receptor 1/2 (VEGFR1/2), vascular endothelial (VE)-cadherin, and matrix metalloproteinases (MMPs).[18,19] Furthermore, epithelial-mesenchymal transition (EMT) is considered a potential mechanism in VM formation and tumor metastasis.[20,21] VM formation is associated with tumor progression, invasion, and poor prognosis in CRC patients.[22,23] However, the relationship between microbial metabolite DCA and VM in intestinal carcinogenesis has not been elucidated.

Due to the vital role of VM in CRC progression, we investigated whether DCA could promote VM, thereby contributing significantly to CRC both in vitro and in vivo. We found that an HFD promoted VM formation and EMT in CRC patients. An HFD modulated gut microbiota and increased the fecal DCA level in $Apc^{min/+}$ mice. Moreover, microbial metabolite DCA increased VM formation by upregulating the VEGFR2 signaling pathway, accompanying with activation of EMT and higher expression of EMT-associated transcription factors, including zinc finger E-box binding homeobox 1/2 (ZEB1/2), thus exacerbating intestinal carcinogenesis. Our study will provide insight into the mechanisms of BA-related intestinal cancer.

TABLE 1 Baseline characteristics of selected patients with colorectal cancer by diet category

Characteristics	High-fat diet (n = 30)	Control diet (n = 30)	P
Male/Female	15/15	15/15	1.000
Age (y)	65 (31-76)	69 (46-78)	.271
BMI			
≥25	12	5	.084
<25	18	25	
History of adenoma	3	1	.612
Family history			.612
Cancer	2	1	1.000
Adenoma	0	2	.492
Smoking			.817
Current	6	8	.761
Former	2	1	1.000
Never	22	21	1.000
Alcohol consumption (≥3 times/wk)	3	3	1.000
Tea consumption (≥3 times/wk)	9	7	.771
Coffee consumption (≥3 times/wk)	3	4	1.000
TNM stage II/III/IV	8/10/12	8/10/12	1.000

2 | MATERIALS AND METHODS

2.1 | Clinical sample collection and trial

A retrospective cohort study was conducted to investigate the VM of CRC patients with or without an HFD. If an individual's average daily intake of red meat has exceeded 100 g over the past year, their diet is considered an HFD.[24,25] A total of 2338 subjects, who underwent a colonoscopy in the digestive endoscopy center of General Hospital, Tianjin Medical University from 2016 to 2018, participated in this study. The patients were divided into an HFD group and a normal diet (ND) group according to the registry before colonoscopy. Advanced CRC was detected in 55 patients in the HFD group and 125 patients in the ND group. Then, we randomly selected 60 CRC patients from the HFD group (n = 30) and the ND group (n = 30), with no significant differences in age, sex, smoking, drinking, and family history of CRC. Human colonic biopsies were obtained to detect vimentin and E-cadherin by immunohistochemistry staining and to evaluate the VM formation by CD34/PAS double-staining. All patients provided informed consent, and the protocol for the study was approved by the ethics committee of General Hospital, Tianjin Medical University, China. The baseline characteristics of selected patients with CRC by diet category are listed in Table 1.

2.2 | CD34/PAS double staining and vasculogenic mimicry identification

CD34/PAS double staining is a method commonly used to verify the formation of VM in tumor tissue.[26] Briefly, after immunohistochemical staining for CD34 (Abcam, 1:100 dilution) was completed, sections were stained with periodic acid solution for 10 minutes, then rinsed twice with distilled water for 3 minutes. Then schiff solution was applied to the sections for 20 minutes prior to rinsing with distilled water, counterstaining with hematoxylin, and dehydrating with ethanol gradient. Finally, sections were mounted using rhamsan gum. To quantify the VM density differences, we calculated the mean number of positive VM channels in five random fields for each tumor site under the microscope (Leica). Then, the average number of each group was used for statistical analysis. The VM[+] channels lined with tumor cells were PAS-positive and CD34-negative and partly contained red blood cells. In addition, traditional vascular channels, lined with endothelial cells rather than tumor cells, were both positive for CD34 and PAS staining. The sections were examined by an experienced pathologist, who was blinded to patient information.

2.3 | Animal treatment and tissue collection

The 4-week-old female $Apc^{min/+}$ mice were purchased from Model Animal Research Center of Nanjing University, China. Mice were kept in a specific pathogen-free (SPF) animal facility at Tianjin Medical University. Twenty $Apc^{min/+}$ mice were equally randomized into an ND group (16% fat, 20% protein, and 64% carbohydrates. n = 5) and an HFD group (60% fat, 20% protein, and 20% carbohydrates. n = 8).[27] After 12 weeks of feeding, the feces were collected for BA analysis.

Four-week-old $Apc^{min/+}$ mice were randomly divided into two groups (n = 10) and treated with sterile water (Con group) and 0.2% DCA (Sigma-Aldrich) in sterile water (DCA group) for 12 weeks according to previous studies and our preliminary study.[10-12] Mice were observed daily. Bedding, diet, and water were changed twice a week, and weight was recorded weekly. The mice were killed by inhaling carbon dioxide at 16 weeks of age. Then the small intestine was dissected and divided into proximal, middle, and distal segments; the colorectum was the fourth segment. After rinsing with a cold sterile PBS solution, the intestinal tumor tissues, para-tumor tissues and normal tissues of the proximal of each segment were stored immediately at −80°C, respectively. All animal experimental procedures were approved by the Institutional Animal Care and Use Committee of Tianjin Medical University, Tianjin, China.

2.4 | 16S rRNA amplicon sequencing

The 16S rRNA gene sequencing used to analyze the gut microbiota composition was performed by TinyGene Bio-Tech. Total genomic DNA from frozen stool samples was isolated using the QIAamp DNA Stool Mini Kit (Omega Bio-Tek). All quantified amplicons were pooled to equalize concentrations for sequencing using 2 × 300 v3 sequencing chemistry on the Illumina MiSeq platform. The high-quality reads were clustered into operational taxonomic units (OTUs) based on sequences with ≥97% similarity and then analyzed using Mothur (version v.1.30.1). Similarly, alpha/beta diversity and rank abundance curve analyses were implemented by Mothur (version v.1.30.1). Linear discriminant analysis of the effect size (LEfSe) and rank sum test (R version) were used to screen different species and functions.

2.5 | Analysis of bile acids

The fecal BA profiles were obtained using liquid chromatography-mass spectrometry.[28] The samples were completely crushed, reconstituted with chromatographic ethanol, ultrasonically treated for 1 hour at 30°C, then centrifuged at 10 000 _g_ for 10 minutes at 4°C. The supernatant of feces was applied to quantify the concentrations of BAs via a liquid chromatograph (Agilent 1260) coupled to a 6120B mass spectrometer using an external standard method. Correlation between the fecal BA concentrations and abundance of gut microbiota was analyzed based on Spearman's correlation coefficients. The heat map showing the correlation matrix between BAs and gut bacteria was generated with the pheatmap package of R software, and the significance was determined by _P_ value ($P < .05$ represented a significant correlation). Red cells represent a positive correlation and blue cells represent a negative correlation.

2.6 | Histological and immunohistochemical analyses

The sections were submitted for histopathological analysis according to standard hematoxylin and eosin (H&E) staining protocols. Pathology was further evaluated by a senior pathologist who was blind to the groups. For immunohistochemistry, the tissue slides were incubated with the following primary antibodies: rabbit polyclonal anti–ki67 (Abcam, 1:200), rabbit polyclonal anti–vimentin (Affinity, 1:400), rabbit polyclonal anti–E-cadherin (Cell Signaling Technology, 1:400), rabbit polyclonal anti–p-VEGFR2 (Abcam, 1:400), and rabbit monoclonal anti–β-catenin (Cell Signaling Technology, 1:100). Sections were incubated with secondary antibodies linked to horseradish peroxidase (HRP) and were then counterstained with hematoxylin.

The E-cadherin expression was mainly localized in the cell membranes of epithelial cells with continuous linear distribution; however, the vimentin expression was mainly located in the cytoplasm of mesenchymal cells, distributed in sheets or nests. The p-VEGFR2 expression was predominantly expressed in the cell membranes and cytoplasm of endothelial cells. The β-catenin expression was localized in cell membrane under normal conditions; ectopic β-catenin

expression was located in the cytoplasm and nucleus; and cells with ectopic expression were defined as positive cells. The tumor area was identified at low magnification, and then the representative photographs were acquired under the high magnification. The percentage of positive cells was obtained based on the mean value from five random fields in each slice. Image J was used for immunohistochemical analysis.

2.7 | TUNEL assay

The TUNEL assay was used to detect tumor cellular apoptosis, which was performed with a commercially available kit (Roche Applied Science) according to the manufacturer's instructions. The apoptotic index was calculated as the percentage of positive cells in randomly selected tumor fields under a fluorescence microscope.

2.8 | Real-time PCR analysis

The intestinal tumor tissues isolated from mice or the cell lysates of cancer cells were directly homogenized in TRIzol Reagent (Ambion, cat #15596026), then total RNA was extracted with an RNeasy Mini Kit (Qiagen) according to the manufacturer's instructions. cDNA was synthesized from RNA using the TIANScript RT Kit (TIANGEN). The relative mRNA expression levels of the target genes were quantified using the standard $2^{-\Delta\Delta Ct}$ method. The oligonucleotide primers for target genes are listed in Table 2.

2.9 | Western blot analysis

Total proteins were extracted using RIPA buffer supplemented with proteinase inhibitor and phosphatase inhibitor (Solarbio). The membranes were then incubated with specific primary antibodies, including anti–VE-cadherin (Abcam, 1:1000), anti–E-cadherin (Cell Signaling Technology, 1:1000), anti–vimentin (Affinity, 1:1000), anti–VEGFR2 (Cell Signaling Technology, 1:1000), anti–phospho-VEGFR2 (Abcam, 1:1000), anti–GAPDH (Affinity, 1:3000), and anti–β-actin (Cell Signaling Technology, 1:1000) at 4°C overnight. After binding HRP-conjugated secondary antibodies (Cell Signaling Technology, 1:5000), the individual protein bands were visualized by enhanced chemiluminescence. Then the relative density of the bands was quantified by Image J.

2.10 | Cell culture

The human CRC cells (HCT-116) were purchased from the American Type Culture Collection (ATCC). HCT-116 cells were incubated in DMEM supplemented with 10% FBS and 1% penicillin-streptomycin solution, and maintained in a humidified atmosphere containing 5%

TABLE 2 Primer sequences used for real-time PCR

Primers	Sequence
Mouse sequences:	
GAPDH	Forward 5'-GGAGAAACCTGCCAAGTATG-3'
	Reverse 5'-TGGGAGTTGCTGTTGAAGTC-3'
E-cadherin	Forward 5'-GACCAGTTTTCTCGTCCATGC-3'
	Reverse 5'-AAGCTGGGAAACGTGAGCAG-3'
Vimentin	Forward 5'-TTTCTCTGCCTCTGCCAAC-3'
	Reverse 5'-TCTCATTGATCACCTGTCCATC-3'
Claudin-4	Forward 5'-GTTCATCGTGGCAAGCATG-3'
	Reverse 5'-CCATAGGGTTGTAGAAGTCGC-3'
Fibronectin	Forward 5'-CTTTGGCAGTGGTCATTTCAG-3'
	Reverse 5'-ATTCTCCCTTTCCATTCCCG-3'
VEGFR-1	Forward 5'-GAGCCAGGAACATATACACAGG-3'
	Reverse 5'-GCTTGACAGTCTAAGGTCGTAG-3'
VEGFR-2	Forward 5'-ATAGAAGGTGCCCAGGAAAAG-3'
	Reverse 5'-TCTTCAGTTCCCCTTCATTGG-3'
VE-cadherin	Forward 5'-CAGCAACTTCACCCTCATAAAC-3'
	Reverse 5'-TCCCGATTAAACTGCCCATAC-3'
ZEB1	Forward 5'-AGACTATTCTGATTCCCCAAGTG-3'
	Reverse 5'-CCTTCTGAGCTAGTGTCTTGTC-3'
ZEB2	Forward 5'-GGAGCTAAGGGAGAGTGTTG-3'
	Reverse 5'-AATTGTGGTCTGGATCGTGG-3'
Human sequences:	
GAPDH	Forward 5'-ACATCGCTCAGACACCATG-3'
	Reverse 5'-TGTAGTTGAGGTCAATGAAGGG-3'
E-cadherin	Forward 5'-CAGCCTATTTTTCCCTCGACAC-3'
	Reverse 5'-GGCCTTTTGACTGTAATCACACC-3'
Vimentin	Forward 5'-GGAGAAACCTGCCAAGTATG-3'
	Reverse 5'-TGGGAGTTGCTGTTGAAGTC-3'
ZEB2	Forward 5'-GCCATCTGATCCGCTCTTATC-3'
	Reverse 5'-ACCTGTGTCCACTACATTGTC-3'

VEGFR1, vascular endothelial growth factor receptor 1; VEGFR2, vascular endothelial growth factor receptor 2; VE-cadherin, vascular endothelial-cadherin; ZEB1/2, zinc finger E-box binding homeobox 1/2.

CO_2 at 37°C. HCT-116 cells were treated with different concentrations of DCA to evaluate the cell proliferation.

2.11 | Cell Counting Kit-8 cell proliferation assay

HCT-116 cells (2000 cells per well) were seeded in 96-well plates. Five parallel holes were set in each group. The cell viability was determined after 0, 24, 48, and 72 hours of treatment with different concentrations of DCA using a Cell Counting Kit-8 (CCK-8, Beyotime) according to the manufacturer's instructions. Briefly, at

every test point, 10 μL CCK-8 reagent was added to each well and incubated at 37°C for 2 hours, and the absorbance was measured with a microplate reader at the wavelength of 450 nm to evaluate the cell viability.

2.12 | Three-dimensional culture assay

Vasculogenic mimicry formation was detected using 3D culture containing Matrigel (BD) in vitro.[29,30] The 24-well plates were coated with 50 μL Matrigel and allowed to solidify for 1 hour at 37°C for subsequent experiments. After stimulation with 20 μM DCA or treatment with DCA with transfection of VEGFR2 siRNA, the HCT-116 cells were seeded on the plate covered with solidified Matrigel at a concentration of $5 \times 10.^5$ The tube-like structures were captured under an inverted microscope after 6 hours of incubation, and the number of complete VM structures in each group was quantified and analyzed.

2.13 | Wound healing assay

HCT-116 cells were incubated overnight in 48-well plates and formed uniform monolayer cells that were at least 90% fused. The 200-μL sterile pipette tip was applied to generate an artificial wound in the center of the well plate covered with cells. The cells were treated with DCA at a concentration of 20 μM or equivalent volume of DMSO (control) for 24 hours. Each group was provided with 4/5 parallel repeating wells. The wound closure in the same position was captured by inverted microscope (magnification 40×) at 0, 12, and 24 hours after the scratch. Image J was used to measure the wound area of cells. The percentage of wound healing migration of HCT-116 cells was calculated with 0% of the wound closure rate at 0 hour as a reference.

2.14 | Knockdown of vascular endothelial growth factor receptor 2 in HCT-116 cells

Gene silencing of VEGFR2 in HCT-116 cells was performed as described previously.[31] Small interfering RNA (siRNA) targeting VEGFR2 (VEGFR2 siRNA: sense strand, 5′-CUCGGUCA UUUAUGUCUAUTT-3′, antisense strand, 5′-AUAGACAUAAAU GACCGAGTT-3′) and control siRNA (non–targeting siRNA: sense strand, 5′-UUCUUCGAACGUGUCACGUTT-3′, antisense strand, 5′-ACGUGACACGUUCGGAGAATT-3′) were purchased from GenePharma. VEGFR2 siRNA or control siRNA was introduced into HCT-116 cells using Lipofectamine 2000 (Invitrogen) in Opti-MEM. After a 6-hour incubation, the medium was replaced with complete medium in the presence or absence of 20 μM DCA for 24 hours to evaluate the EMT process, tube formation, migration, and VEGFR2 signaling molecule.

2.15 | Statistical analysis

All data are shown as the mean ± standard deviation (SD). The comparison was performed using Student's *t* test across two groups and one-way ANOVA for multiple comparisons. Statistical analysis was performed on GraphPad Prism 7.0 (GraphPad Software). All experiments were repeated in triplicate, and $P < .05$ was deemed statistically significant.

3 | RESULTS

3.1 | High-fat diet exacerbated the vasculogenic mimicry formation and epithelial-mesenchymal transition process in colorectal cancer patients

A growing body of evidence supports that VM is closely associated with an HFD. A cohort study showed that the serum low-density lipoprotein levels of CRC patients with liver metastases were significantly higher than those of CRC patients without liver metastases.[32] Moreover, an HFD could increase colon cancer cell proliferation, tumor angiogenesis, and lung metastasis in mice.[33,34] To understand the association between HFD and CRC progression, we investigated the effect of an HFD on VM and EMT in CRC patients. We found that the number of positive VM channels was significantly higher in CRC patients with an HFD compared to CRC patients with an ND (Figure 1A). In addition, immunohistochemistry showed that an HFD reduced the E-cadherin expression level and elevated the expression of vimentin (Figure 1B,C), which served as epithelial markers and mesenchymal markers, respectively. These results suggested that an HFD could be closely related to the EMT process and VM formation in CRC.

3.2 | High-fat diet altered the composition of the gut microbiota and fecal bile acid profile of $Apc^{min/+}$ mice

It is known that an HFD could induce gut microbiota dysbiosis in mice.[5,35] To determine the changes in the gut microbiome of the ND group and the HFD groups, we used 16S rRNA-based high-throughput sequencing technology to ascertain the composition of the mouse fecal microbiome. The unique and shared OTUs of different groups were determined using a Venn diagram (Figure 2A). There are 276 OTUs in the HFD group and 307 OTUs in the ND group, with 222 shared OTUs. When principal component analysis (PCA) was used to analyze the differences between the two groups, the gut microbiota composition in each group showed an obvious aggregation and was not similar (Figure 2B). At the phylum level, the microbiota community composition between the two groups was different. In the HFD group, the relative abundance of *Firmicutes* and *Actinobacteria* were elevated with the reduction of *Bacteroidetes*, and the *Firmicutes/Bacteroidetes* ratio was increased simultaneously
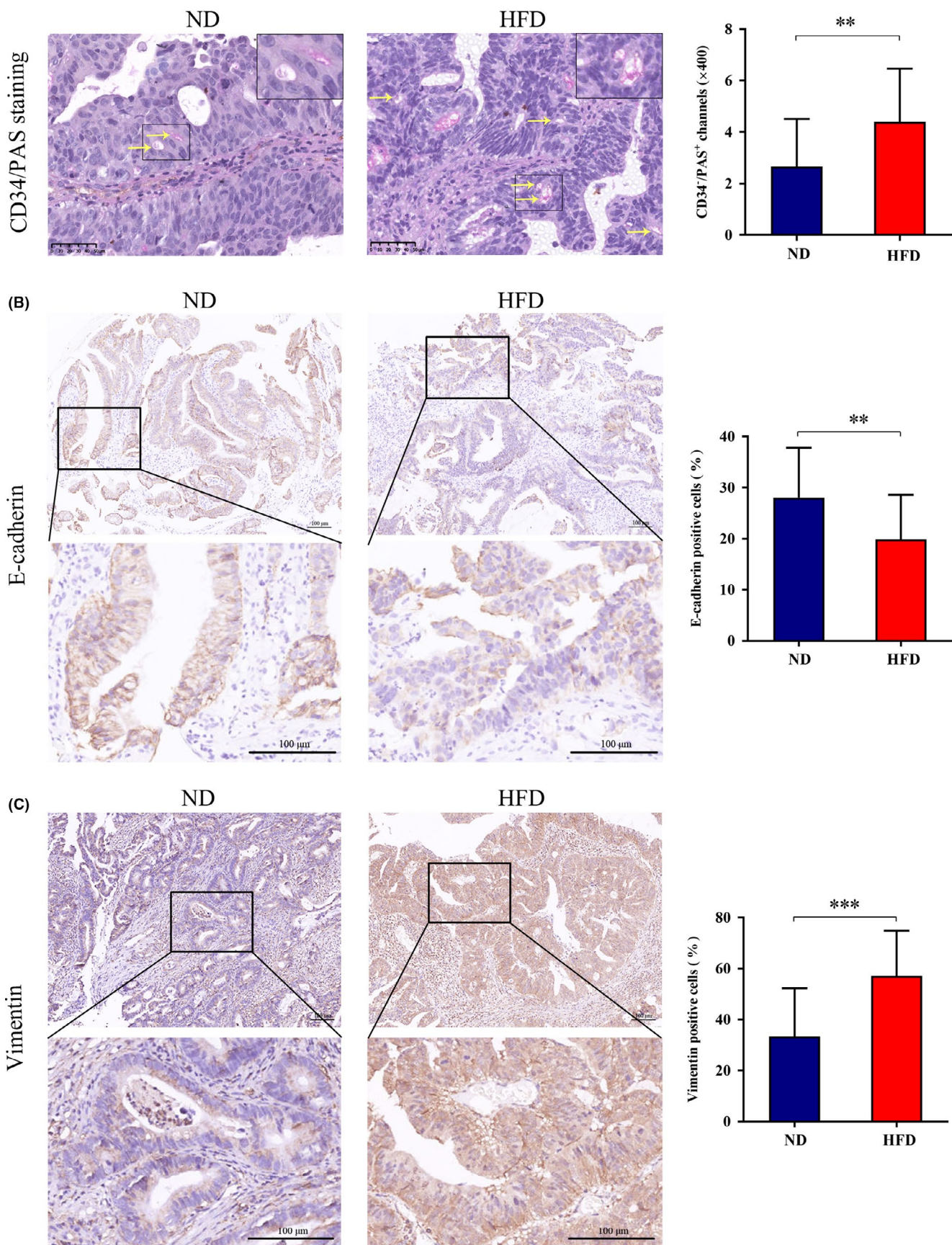
(A) CRC patients

(B)

(C)

FIGURE 1   Legend on next page

FIGURE 1 A high-fat diet exacerbated vasculogenic mimicry formation in patients with colorectal cancer. A, CD34/PAS double staining was used to identify vasculogenic mimicry (VM) and endothelium-dependent vessels. The yellow arrow pointed to the VM$^+$ channels (PAS-positive and CD34-negative channels). Scale bars: 50 µm. B and C, Immunohistochemical staining was used to distinguishing EMT-related markers (E-cadherin and vimentin) between the ND and HFD groups. Scale bars: 100 µm. **$P < .01$, ***$P < .001$. n = 30 for each group

(Figure 2C). We then used the Chao index to reveal a lower bacterial richness in HFD-fed mice compared with ND-fed mice (Figure 2D). The analysis of similarities (ANOSIM) and heat map representing the β diversity revealed significant differences between the two groups (Figure 2E,F). Next, LEfSe analysis was used to estimate the differentially abundant species between the ND group and the HFD group. The mice with a HFD had higher levels of opportunistic pathogens, including *Enterococcus*, *Streptococcus*, *Lachnoclostridium*, *Alistipes*, and *Desulfovibrio*. In contrast, beneficial bacteria, such as *Candidatus* Arthromitus, *Marvinbryantia*, and *Parasutterella*, were relatively less abundant in the HFD group compared with the ND group (Figure 2G).

To investigate the dynamic changes of fecal BAs induced by HFD intervention, liquid chromatography-mass spectrometry was used to quantitatively analyze the BAs in feces. As shown in Figure 2H, the HFD led to disproportionate increases in primary BAs and obvious increases in secondary BAs in *Apc*$^{min/+}$ mice. In particular, the feces DCA level in the HFD group increased over 600-fold. We further explored the relationship between the BA profile and gut microbiota composition through Spearman correlation analysis (Figure 2I). Interestingly, *Mucispirillum*, *Blautia*, *Lactobacillus*, *Parabacteroides*, *Enterococcus*, *Escherichia*, and *Streptococcus* were positively correlated with secondary BAs, such as DCA, wMCA, HDCA, LCA, TDCA, 6-ketoLCA, and NorDCA, while negatively correlated with primary BAs, such as TUDCA, CDCA, CA, TaMCA, and TbMCA. More importantly, these microbial genera share a common function of forming the bile salt hydrolases (BSH), which catalyze the hydrolysis of the conjugated primary BAs. Most of these microbes were more abundant in the HFD group. Collectively, these data suggested that an HFD was significant in modulating gut microbiota and disturbing BA metabolism. Especially, DCA was the most obvious change in the BA profile, which may be associated with a significant influence on the occurrence and development of HFD-induced CRC.

3.3 | High-fat diet-induced microbial metabolite deoxycholic acid accelerated carcinogenesis in *Apc*$^{min/+}$ mice

Further studies were conducted to determine whether DCA alone is sufficient to induce similar effects of an HFD (Figure 3A). There was no difference in the life status after DCA treatment, and none of the mice died. With no difference in food intake, there was a gradual increase in weight in both groups, but no difference was found ($P > .05$, Figure 3A). The average number of tumors was increased by approximately 1.6-fold (11.10 ± 0.90 vs 18.30 ± 1.21, $P < .001$) and 2.6-fold (0.70 ± 0.26 vs 1.80 ± 0.29, $P < .05$) in the small intestine

and colon of the DCA group, respectively (Figure 3B). Meanwhile, the number of tumors of each segment of the small intestine in the DCA group was significantly increased compared with the control group (Figure 3C). Moreover, the number of tumors of various sizes was increasing in the DCA group, mainly those with diameters of 1-2 mm and >2 mm (1-2 mm: 4.80 ± 0.61 vs 8.00 ± 0.77, $P < .01$; >2 mm: 1.10 ± 0.31 vs 3.80 ± 0.63, $P < .01$, Figure 3D). More importantly, morphology showed that only a few scattered small polyps were observed in the control group, while larger tumors, especially in the colon, were observed in the DCA group (Figure 3E). Histopathologically, among DCA-treated mice, 70% (7/10) were confirmed to have high grade dysplasia (HGD) or intramucosal carcinoma, whereas only 20% (2/10) of the control group was considered to have HGD or intramucosal carcinoma, and another 40% (4/10) was found to have low grade dysplasia (LGD; Figure 3F). Collectively, these results demonstrated that DCA could promote intestinal carcinogenesis.

3.4 | Deoxycholic acid-induced proliferation and inhibited apoptosis in intestinal epithelial cells of *Apc*$^{min/+}$ mice

To better understand the effect of DCA on tumor progression, we further detected the proliferation and apoptosis in intestinal tumor tissues. The percentage of Ki-67 positive cells of the DCA group was increased significantly ($28.12\% \pm 2.57\%$ vs $51.9\% \pm 3.60\%$, $P < .001$ Figure 4A). Meanwhile, the number of apoptotic cells, detected by TUNEL assay, was decreased in the DCA group compared with the control group ($15.90\% \pm 1.62\%$ vs $9.20\% \pm 1.26\%$, $P < .01$, Figure 4B). The status of β-catenin was also significantly increased in the DCA group, suggesting that DCA could promote tumor cell proliferation (Figure 4C). These findings supported that DCA promoted proliferation, reduced apoptosis, and accelerated the intestinal adenoma-to-adenocarcinoma sequence.
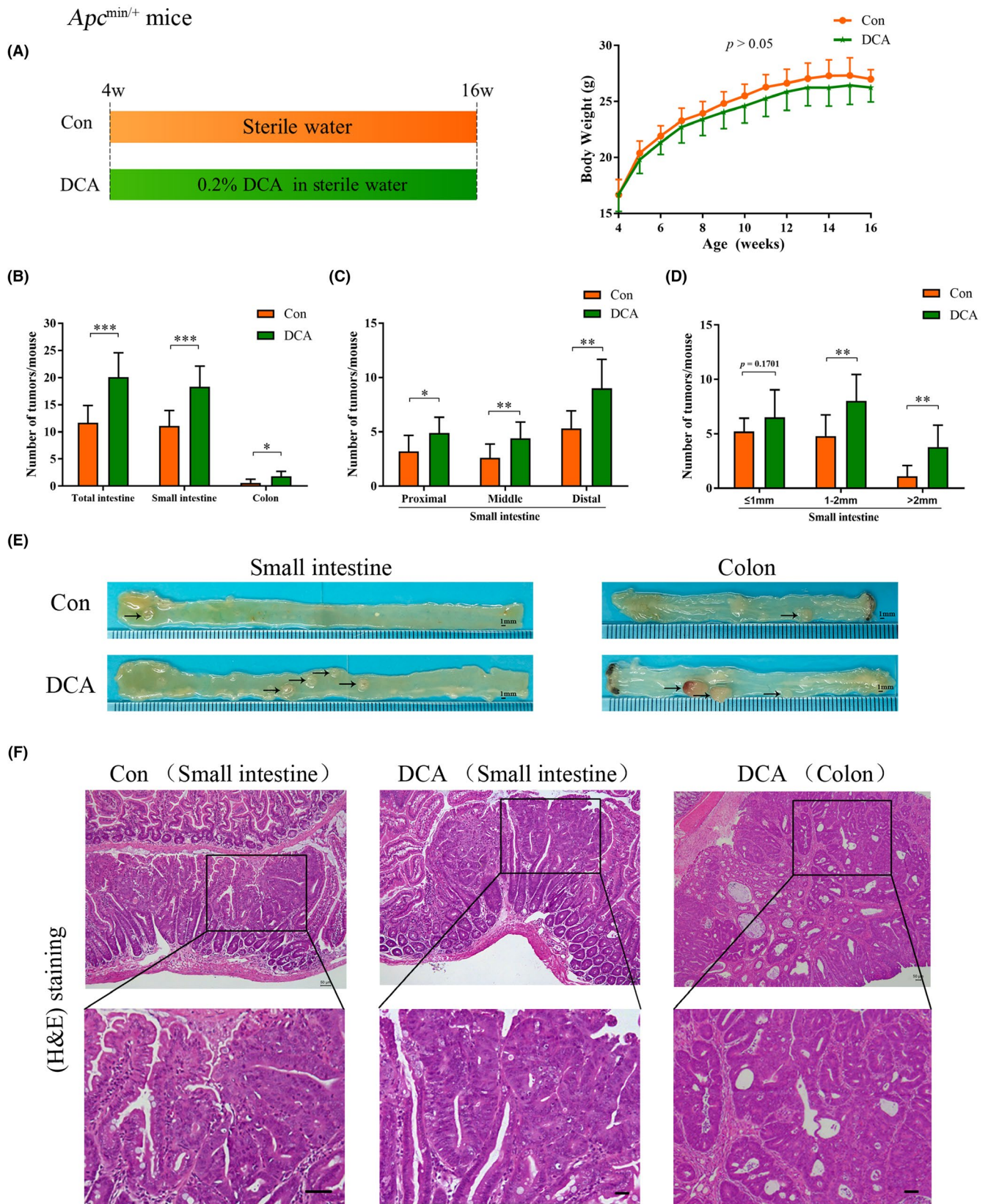
3.5 | Deoxycholic acid drove vasculogenic mimicry formation and the epithelial-mesenchymal transition process in *Apc*$^{min/+}$ mice

After identifying that DCA could promote the malignant progression of intestinal tumors in *Apc*$^{min/+}$ mice, we investigated the relationship between DCA and VM formation, which is closely related to intestinal tumor progression. In contrast to the control group, the DCA group had a higher number of VM channels, which were lined with tumor cells rather than endothelial cells (Figure 5A). VE-cadherin, as a trans-membrane protein responsible for cell-cell adhesion, is

FIGURE 2 High-fat diet altered the composition of the gut microbiota and fecal bile acid profile of $Apc^{min/+}$ mice. A, Venn diagram. B, Principal component analysis (PCA) of fecal bacteria in two groups. C, Differences in microbial community composition between the two groups at phylum level. D, Chao index. E, ANOSIM analysis based on weighted UniFrac distances. F, The heat map showed a clear difference. G, Differentially abundant species in the cladogram generated by linear discriminant analysis of the effect size (LEfSe). H, Fecal bile acids (BAs) levels in $Apc^{min/+}$ mice treated with ND or HFD were detected, showing that deoxycholic acid (DCA) was significantly higher in the HFD. I, Spearman correlation analysis between several significantly changed fecal BAs and genera bacteria. $^*P < .05$, $^{**}P < .01$, $^{***}P < .001$. ND, n = 5; HFD, n = 8

FIGURE 3 Deoxycholic acid accelerated intestinal adenoma-adenocarcinoma sequence in $Apc^{min/+}$ mice. A, Experimental flow chart of $Apc^{min/+}$ mice drinking sterile water or sterile water containing 0.2% DCA for 12 weeks. There was no significant difference in body weight between the DCA group and the control group. B, The total number of intestinal tumors per mouse was increased in the DCA group. C and D, In the DCA group, the number and size of tumors in the proximal, middle and distal small intestine increased markedly. E, The representative macroscopic images of tumors were shown in the small intestine and colon of the two groups. F, HE staining. *$P < .05$, **$P < .01$, ***$P < .001$. n = 10 for each group

positively correlated with VM formation.[36] DCA treatment increased VE-cadherin both at the mRNA and protein levels (Figure 5B-D).

Compared with the control group, DCA had significantly suppressed the expression of epithelial markers (claudin-4 and E-cadherin), as well as increased the expression of mesenchymal markers (vimentin and fibronectin; Figure 6A,B). The expressions of the EMT-associated proteins, including E-cadherin and vimentin, were also detected using western blot analysis, and the results
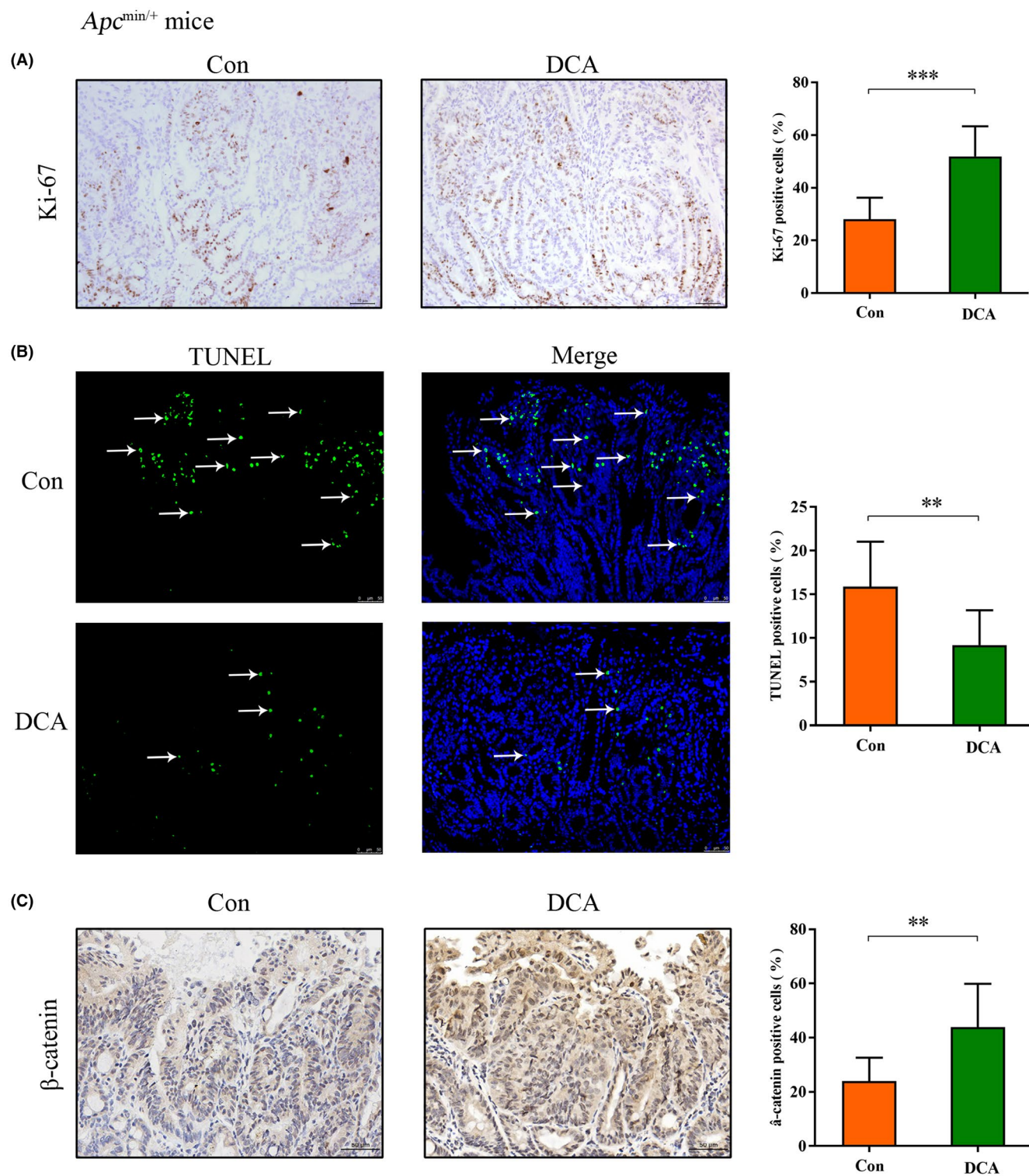
FIGURE 4 Deoxycholic acid promoted proliferation and reduced apoptosis of intestinal tumor cells in $Apc^{min/+}$ mice. A and B, The tumor tissues were randomly selected from each section, and the percentage of positive cells was calculated by Ki-67 and TUNEL staining. (C) The β-catenin expression in the intestinal tumors was assessed by immunohistochemical staining. Scale bars: 50 μm. **$P < .01$, ***$P < .001$. n = 10 for each group

were similar to those for real-time PCR (Figure 6C,D). As shown in Figure 6E, the immunohistochemistry staining demonstrated that DCA decreased the expression of E-cadherin and increased the expression of vimentin, consistent with the above analysis. Collectively, these results suggested that DCA could promote VM formation and induce EMT in $Apc^{min/+}$ mice.

3.6 | Deoxycholic acid accelerated the epithelial-mesenchymal transition process, vasculogenic mimicry formation, and migration in HCT-116 cells

HCT-116 cells were treated with DCA at different concentrations (0, 20, 50, 100, and 200 µM) at a certain time gradient (0, 24, 48, 72, and 96 hours). The CCK-8 assay revealed that low concentrations of DCA (<50 µM) promoted cell proliferation, but excessive concentrations of DCA may lead to massive cell necrosis due to toxic effects (Figure 7A). DCA induced EMT in HCT-116 cells in a concentration-dependent and time-dependent manner. In particular, HCT-116 cells treated with 20 µM DCA for 24 hours strongly elevated the expression of vimentin protein and significantly diminished the E-cadherin protein expression level (Figure 7B,C). Then we analyzed the experimental results from the mRNA level, consistent with western blot analysis (Figure 7D). The effect of DCA on VM formation of

HCT-116 cells was investigated using the well-established 3D model in vitro. We found that the HCT-116 cells treated with 20 µM DCA formed more typical and completed vessel-like tubes compared to the control group (Figure 7E). Furthermore, wound healing experiments confirmed that HCT-116 cells treated with 20 µM DCA had a higher migration rate and narrower wound area, showing that DCA promoted cell migration (Figure 7F). In short, DCA accelerated the EMT process, VM formation, and migration in HCT-116 cells, which resulted in tumor cells having more invasive properties and phenotypes.

3.7 | Deoxycholic acid activated the vascular endothelial growth factor receptor 2 signaling pathway in $Apc^{min/+}$ mice

Vascular endothelial growth factor receptor 2 is overexpressed in many cancers and is involved in metastasis and recurrence.[37,38] We found that compared with the control group, the mRNA level of VEGFR2 was markedly elevated in the DCA group; however, no significant change was observed in the level of VEGFR1 (Figure 8A). Considering the contributions of EMT-related transcription factors in EMT, we also measured ZEB1 and ZEB2 mRNA levels in intestinal tumor tissues, which were significantly higher in DCA-treated mice than those in
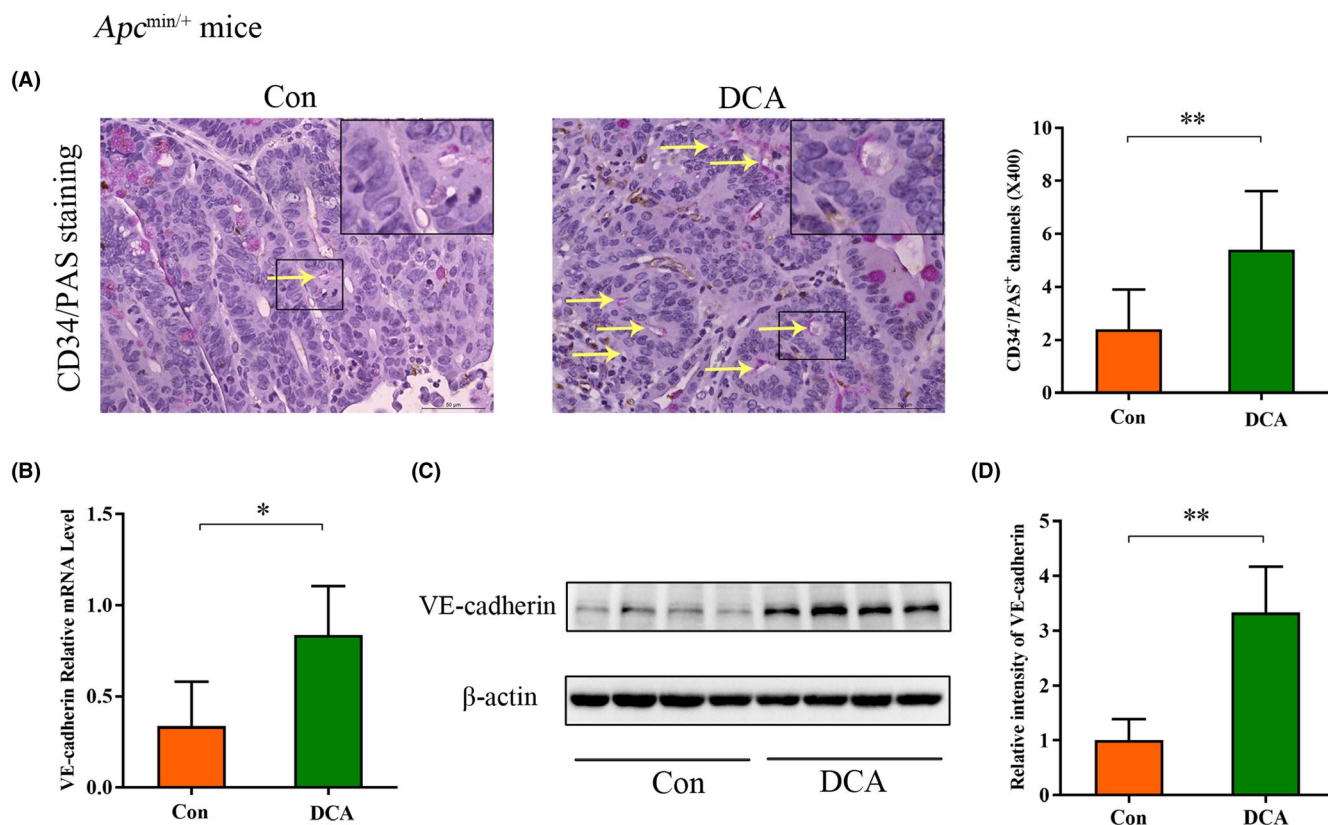
FIGURE 5 Deoxycholic acid (DCA) drove vasculogenic mimicry formation in $Apc^{min/+}$ mice. A, The number of VM+ channels from each tumor tissue was significantly increased in the DCA group. n = 10. B, Relative mRNA level of vasculogenic mimicry (VM)-related marker (vascular endothelial-cadherin [VE-cadherin]) was evaluated by Real-timemPCR. n = 5. C and D, Western blot assay of VE-cadherin showed a higher protein level in the DCA group. n = 4. Scale bars: 50 µm. *P < .05, **P < .01

the control (Figure 8A). Using western blot analysis, we investigated the expression of VEGFR2 and its phosphorylation indices and found that VEGFR2 and p-VEGFR2 were overexpressed in the DCA group

(Figure 8B). The immunohistochemical staining demonstrated that compared with the control mice, the DCA-treated mice showed higher expression of p-VEGFR2 in the intestinal tumors (Figure 8C).
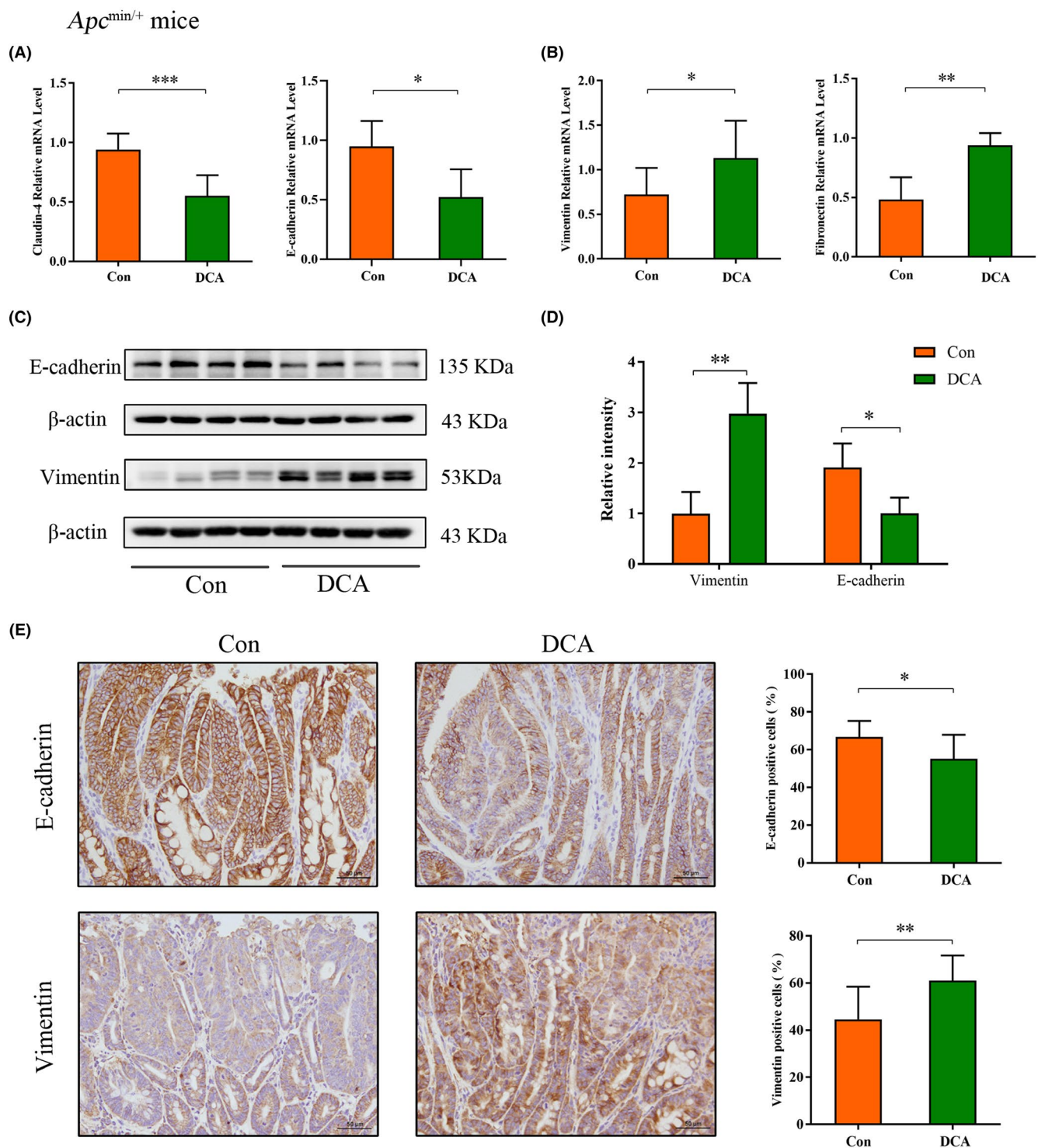
FIGURE 6 Deoxycholic acid (DCA) induced the epithelial-mesenchymal transition in $Apc^{min/+}$ mice. A and B, Real-time PCR analysis revealed DCA downregulated epithelial markers (claudin-4 and E-cadherin) and upregulated mesenchymal markers (vimentin and fibronectin) expression, respectively. C and D, vimentin expression was higher in the DCA group than in the control group, whereas the expression of E-cadherin was decreased. n = 4. E, Immunohistochemical analysis; n = 10 for each group. Scale bars: 50 μm. *P < .05, **P < .01, ***P < .001
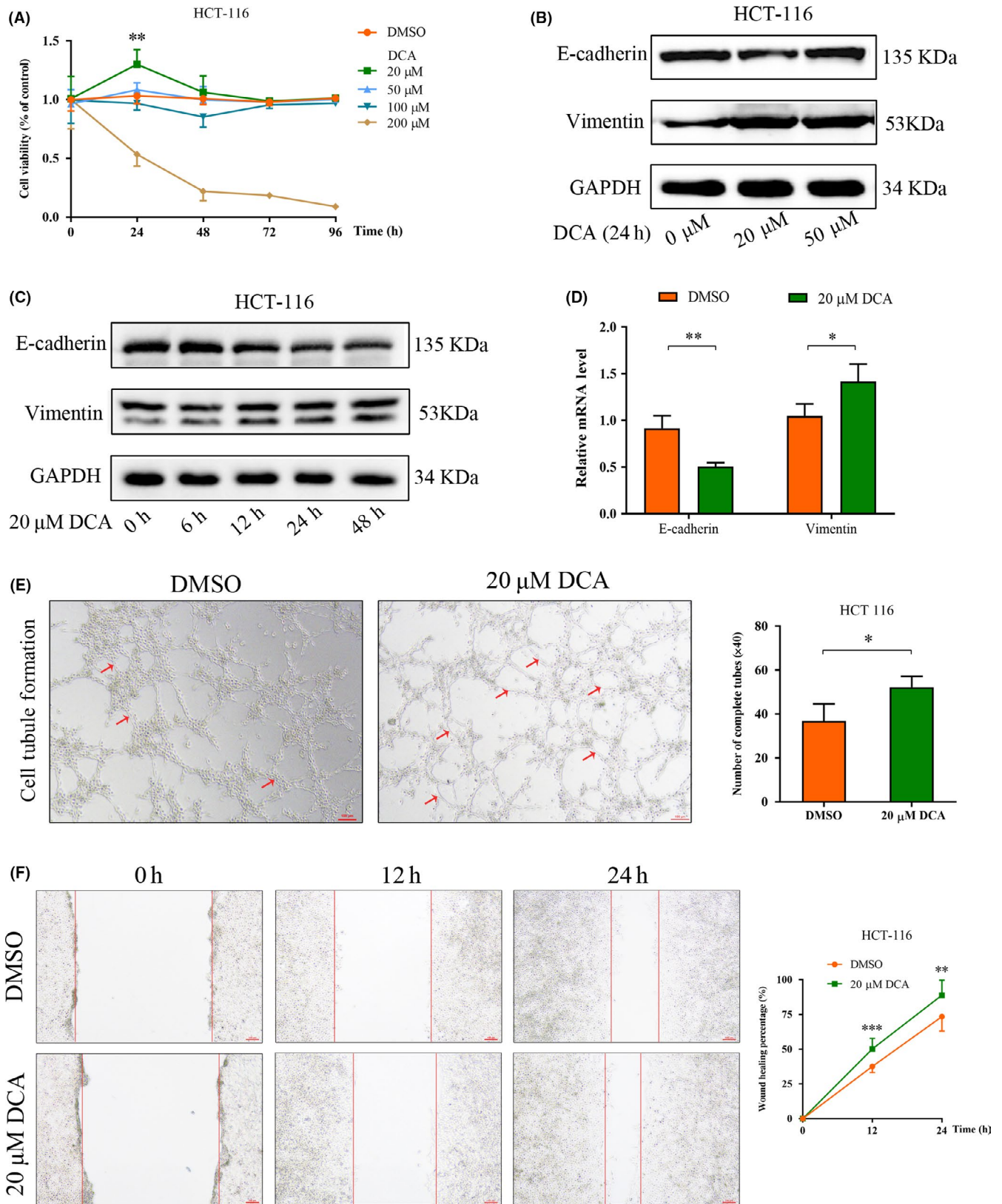
FIGURE 7 Deoxycholic acid (DCA) accelerated vasculogenic mimicry formation, epithelial-mesenchymal transition, and migration in HCT-116 cells. A, The proliferative abilities of HCT-116 cells treated by DCA with different concentrations and time were determined by Cell Counting Kit-8 (CCK-8). B and C, The expression levels of vimentin and E-cadherin proteins were detected in HCT-116 cells treated with DCA, along with concentrations and time variation. D, The mRNA levels of epithelial-mesenchymal transition (EMT) markers in HCT-116 cells treated with DCA. E, The images of vessel-like tubular structures in a three-dimensional culture model are presented. The numbers of corresponding patterned networks were counted under an inverted microscope. F, Wound healing assays suggested that DCA accelerated migration in HCT-116 cells. Quantitative measurements of wound closure were analyzed between the two groups. Scale bars: 100 μm. *$P < .05$, **$P < .01$, ***$P < .001$
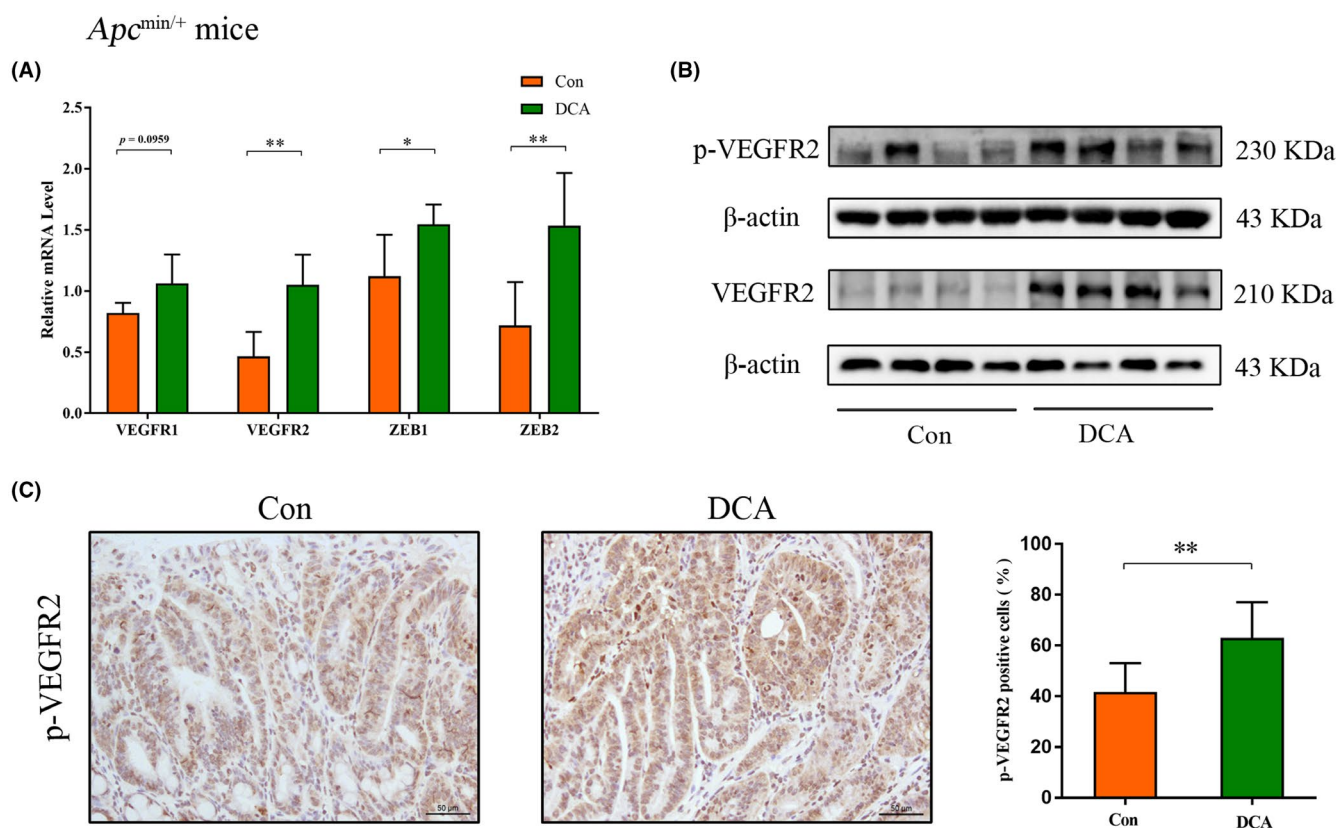
3.8 | Silence of vascular endothelial growth factor receptor 2 affected the deoxycholic acid-induced epithelial-mesenchymal transition process, vasculogenic mimicry formation, and migration in HCT-116 cells

Vascular endothelial growth factor receptor 2 siRNA was trans-fected in HCT-116 cells, using control siRNA as a control, to explore whether VEGFR2 was necessary for the DCA-induced EMT and VM. The transfection efficiency was determined by western blot analysis (Figure 9A). Due to the VEGFR2 transfection, the elevated mRNA expression of ZEB2 in DCA-treated HCT-116 cells was sup-pressed (Figure 9B). Depletion of VEGFR2 reduced the expression of E-cadherin and elevated the vimentin expression level caused by DCA, highlighting the crucial role of VEGFR2 on the DCA-induced EMT process (Figure 9C,D). Moreover, as shown in Figure 9E, the

VEGFR2 knockdown decreased the VM formation induced by DCA in HCT-116 cells on the matrix. Similarly, the migration abil-ity of HCT-116 cells treated with DCA was weakened on account of VEGFR2-downregulation compared to the control siRNA group (Figure 9F). In short, these findings showed that VEGFR2 was vital for DCA-induced EMT and VM formation.
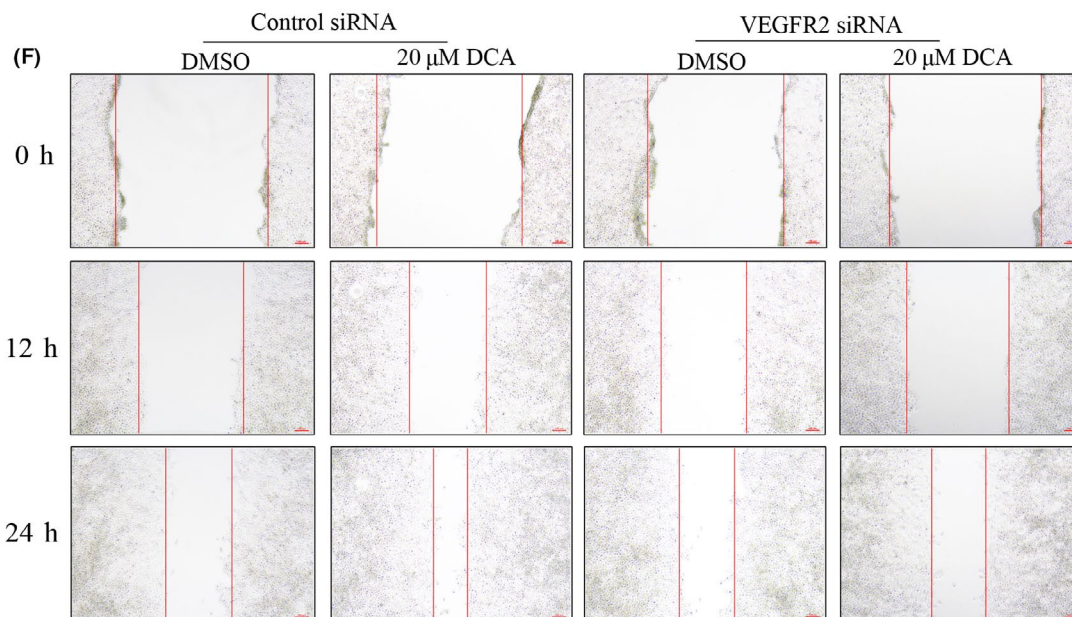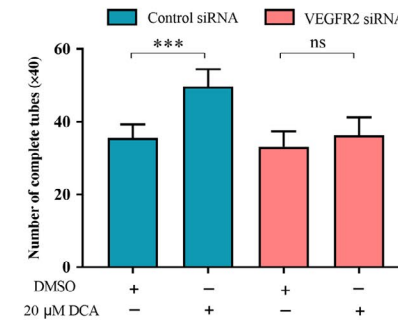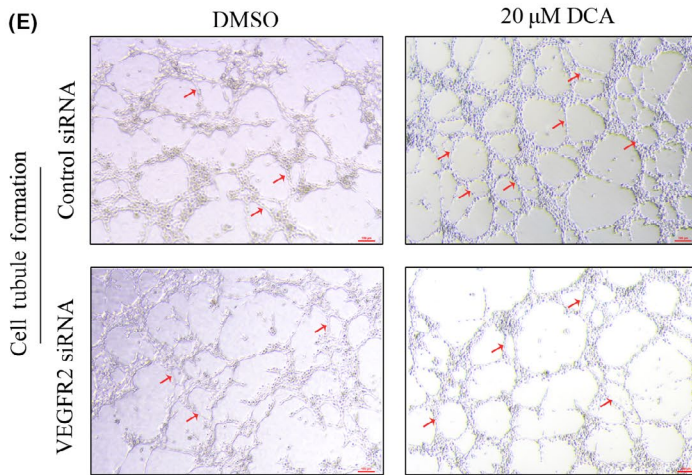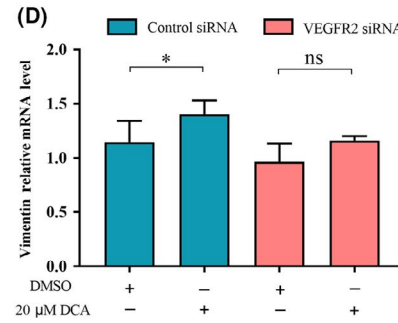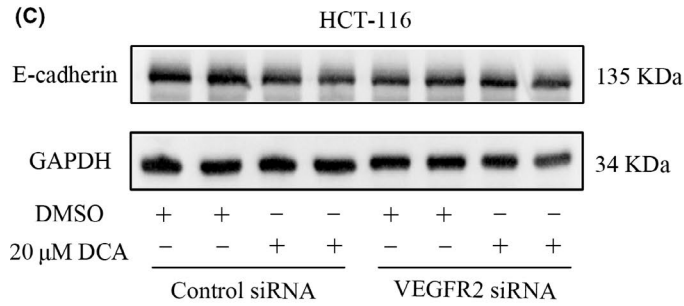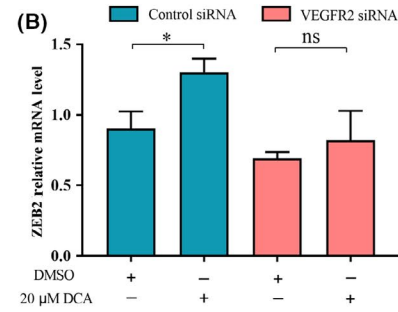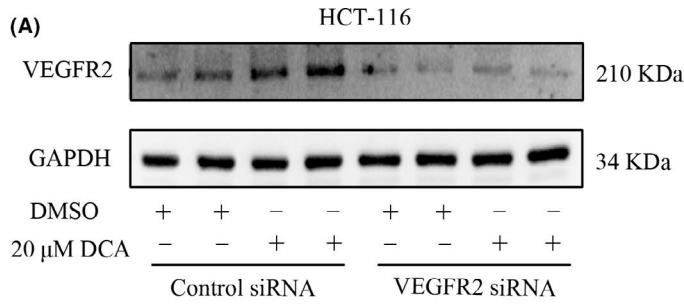
4 | DISCUSSION

Previous studies have revealed that VM refers to the formation of de novo vascular networks by aggressive tumor cells, providing a potential perfusion route for fast-growing tumors and increasing the risk of a poor clinical prognosis.[39,40] Therefore, further research could be conducted to explore the potential carcinogenic risk fac-tors influencing VM formation and the relative mechanisms. In the
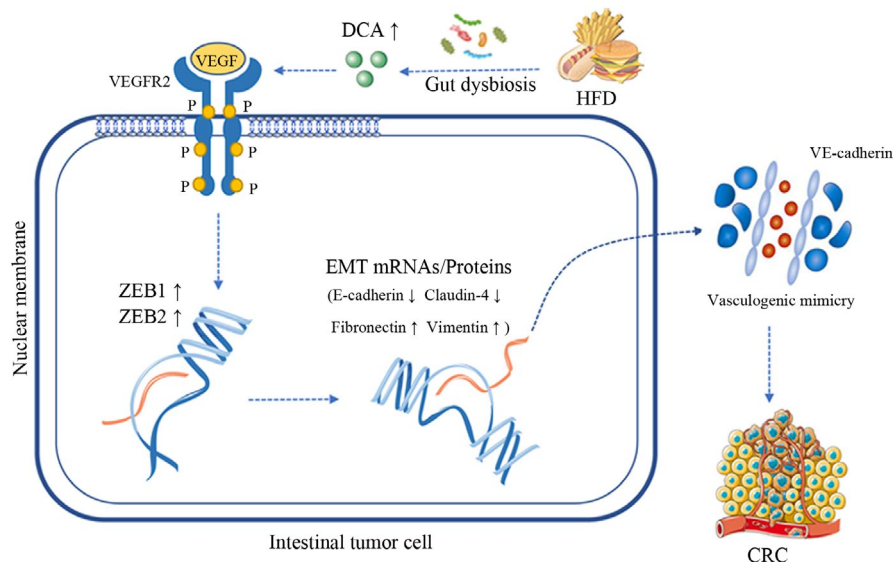

FIGURE 8 Deoxycholic acid (DCA) activated the vascular endothelial growth factor receptor 2 (VEGFR2) signaling pathway in $Apc^{min/+}$ mice. A, The mRNA expression levels of VEGFR1, VEGFR2, ZEB1, and ZEB2 were detected in $Apc^{min/+}$ mice. n = 4-6. B, The expression levels of phosphorylated and total VEGFR2 of intestinal tumor tissues were examined by western blot analysis. n = 4. C, The p-VEGFR2 expression in the intestinal tumors was assessed by immunohistochemical staining, n = 10. Scale bars: 50 μm. *$P < .05$, **$P < .01$

FIGURE 9 Vascular endothelial growth factor receptor 2 (VEGFR2) silencing blunted the deoxycholic acid-induced vasculogenic mimicry formation in HCT-116 cells. A, The transfection effect VEGFR2 siRNA and control siRNA was examined by western blot. B, The mRNA level of epithelial-mesenchymal transition (EMT)-related transcription factors (ZEB2) in different treatment groups. C and D, The mRNA or protein expression of EMT-associated markers (E-cadherin and vimentin) in the HCT-116 cells treated with VEGFR2 siRNA or cntrol siRNA under the condition of DMSO or 20 μM DCA was assessed. E, The forming ability of typical vessel-like tubes of HCT-116 cells after VEGFR2 silencing was examined. The numbers of completed tubes in each image under an inverted microscope were presented. F, Wound healing assays for HCT-116 cells with VEGFR2 knockdown. Quantitative measurements of wound closure are shown. Scale bars: 100 μm. *$P < .05$, ***$P < .001$

(A) HCT-116

VEGFR2 — 210 KDa

GAPDH — 34 KDa

DMSO: + + − − + + − −
20 μM DCA: − − + + − − + +
Control siRNA / VEGFR2 siRNA

(B) ZEB2 relative mRNA level

Control siRNA / VEGFR2 siRNA

(C) HCT-116

E-cadherin — 135 KDa

GAPDH — 34 KDa

DMSO: + + − − + + − −
20 μM DCA: − − + + − − + +
Control siRNA / VEGFR2 siRNA

(D) Vimentin relative mRNA level

Control siRNA / VEGFR2 siRNA

(E) Cell tubule formation

Number of complete tubes (×40)

Control siRNA / VEGFR2 siRNA

(F)
Control siRNA — DMSO / 20 μM DCA
VEGFR2 siRNA — DMSO / 20 μM DCA

0 h

12 h

24 h

FIGURE 10 Microbial metabolite deoxycholic acid promotes vasculogenic mimicry formation of intestinal carcinogenesis by activating vascular endothelial growth factor receptor 2 (VEGFR2) signaling. The schematic model demonstrates the effects of the microbial metabolite DCA on inducing vasculogenic mimicry (VM) and epithelial-mesenchymal transition (EMT) in intestinal epithelial tumor cells. Exposure to microbial metabolite DCA resulted in the activation of VEGFR2, thereby causing the increased expression of epithelial-mesenchymal transition (EMT)-related transcription factors (ZEB1 and ZEB2), which induced EMT and VM formation to promote the intestinal carcinogenesis

present study, we found that an HFD significantly promoted VM formation and EMT in CRC patients, suggesting a link among diet, VM, and CRC.

Studies have suggested that an HFD promotes colorectal tumorigenesis by gut microbiota dysbiosis and alterations in microbiota-related metabolites.[5,35,41] Consistent with this, we revealed that HFD-fed $Apc^{min/+}$ mice exhibited a distinct composition and diversity of gut microbiota, which altered the production of microbe-derived metabolites in the GI tract. BAs are a class of metabolites representing gut microbiota-host co–metabolism. Chronic consumption of an HFD induces an abnormal BA metabolism. As demonstrated in our study, an HFD resulted in disproportionate changes in BAs. Fecal DCA was obviously increased in $Apc^{min/+}$ mice. Therefore, the increased level of fecal DCA induced by an HFD might be involved in the progression of intestinal tumors.

Different from angiogenesis, VM is a non–endothelium-dependent channel-like structure lined with tumor cells.[18] In the past, VM was mainly reported in highly aggressive malignancies, such as melanoma, glioblastoma, hepatocellular carcinoma, and breast cancer.[13,42,43,44] Recently, VM formation in CRC has received more attention in the literatures.[45,46] Traditional antiangiogenic therapies have not sufficiently satisfied the clinical expectations in terms of patient survival and efficacy, in part due to the inherent and acquired resistance to treatment.[47] More importantly, the tumor cunningly deploys alternative flow patterns (VM), and the hypoxic microenvironment resulting from antiangiogenic therapy may further accelerate the formation of VM.[20] Based on this model, VM may become a novel therapeutic target for the clinical treatment of tumors.[14,20,48] For example, galunisertib, a selective TGF-β receptor kinase inhibitor, could exhibit the effective suppression of VM

formation.[48] R8 modified epirubicin-dihydroartemisinin liposomes have been reported to effactually suppress the VM of tumors.[49] Obviously, whether microbial metabolite DCA could independently promote the VM formation in intestinal carcinogenesis both in vitro and in vivo deserves further investigation. Our study provides the first direct evidence of the effect of microbial metabolite DCA on VM formation of intestinal carcinogenesis. VM provides a new perspective for the clinical treatment of tumors.

Since DCA is an important risk factor for promoting VM formation in intestinal tumors, it is necessary to investigate the specific molecular mechanism of this strong stimulation effect. The mechanisms promoting VM formation are very complex, among which EMT is the most studied.[21,50] EMT is a dynamic dedifferentiation process, where epithelial cells lose their typical epithelial features, such as apical-basal polarity and cell adhesion, and acquire mesenchymal cell traits, such as motility and invasion, by downregulating epithelial genes and upregulating mesenchymal genes.[51,52] EMT, which is involved in biological processes such as embryonic development, organ formation, and tissue regeneration in adults, has received more attention in the past two decades due to its potential role in the development of cancer.[51,53,54] Interestingly, we demonstrated that the HFD or DCA alone could induce a decrease in epithelial markers and an increase in mesenchymal markers. EMT inhibitors (SB431542 and U0126EtOH) distinctly weakened the VM formation ability of HCT-116 and HCT-8 cells,[55] indicating that the EMT process was crucial for VM formation of intestinal tumors. Therefore, we speculated that DCA had a positive effect on VM formation by promoting the EMT process. Consistent with the speculation, we validated that DCA led to VM formation by upregulating the expression of EMT-associated proteins.

Deoxycholic acid appears to be a strong stimulant of the vascular endothelial growth factor (VEGF) expression,[56] which is demonstrated to be a vital pro–angiogenic factor involved in tumor metastasis and angiogenesis.[57] Studies have shown that abnormal secretion of VEGF binds to receptor tyrosine kinases to induce receptor dimerization and phosphorylation, particularly VEGFR1/2, resulting in the process of endothelial regeneration, angiogenesis, and induction of tumor EMT.[58,59] Current studies mainly focus on the relationship between VEGFR2 signaling and tumor angiogenesis, and the important role of VEGFR2 in VM formation has been neglected. In the present study, we demonstrated that VEGFR2 participated in the process of VM formation induced by DCA, providing important targets for VM-based therapy. Sorafenib, a significant anti–VEGFR2 drug, has been confirmed to have an inhibitory effect on VM in canine mammary gland tumors.[60] However, short-term anti–VEGF bevacizumab treatment may promote VM formation by inducing a hypoxic tumor microenvironment, which could play a critical role in tumor invasion and metastasis.[61] Therefore, the inhibitor of the VEGFR2 signaling pathway could potentially be used for new targeted drugs to block the VM formation of intestinal tumors under minimizing the negative influence of the tumor microenvironment and strictly controling medication time.[62]

In summary, our results demonstrated that an HFD led to VM formation and dysregulation of gut microbiota and BA metabolism; DCA increased, which promoted the occurrence and progression of intestinal tumors. More importantly, DCA drove EMT and VM formation by modulating VEGFR2 signaling (Figure 10). Overall, VM formation provided a novel understanding regarding the complex carcinogenic mechanism of DCA and is a potential therapeutic target for individualized CRC treatment. However, we mainly explore the mechanisms by which DCA promotes CRC at the animal and cellular levels. As for the clinical level, there are conflicting data on the association between the serum DCA level and human CRC risk, and no definitive conclusions are available.[8,9,63] Because humans and mice differ strongly in genes, physiological structure, biochemical environment, and intestinal microbiota,[64] the results of mouse model experiments are insufficient to explain the human intestinal flora. Moreover, the research direction is limited with a small sample size. Hence, microbial metabolite DCA-promoted vasculogenic mimicry formation in human intestinal carcinogenesis should be further investigated.

DISCLOSURE

The authors have no conflicts of interest to declare.

ORCID

Hailong Cao https://orcid.org/0000-0002-0147-7826

REFERENCES

1. Siegel RL, Miller KD, Jemal A. Cancer statistics, 2020. *CA Cancer J Clin*. 2020;70:7-30.
2. Low EE, Demb J, Liu L, et al. Risk factors for early-onset colorectal cancer. *Gastroenterology*. 2020;159:492-501.e7.
3. Kerr J, Anderson C, Lippman SM. Physical activity, sedentary behaviour, diet, and cancer: an update and emerging new evidence. *Lancet Oncol*. 2017;18:e457-e471.
4. Huxley RR, Ansary-Moghaddam A, Clifton P, Czernichow S, Parr CL, Woodward M. The impact of dietary and lifestyle risk factors on risk of colorectal cancer: a quantitative overview of the epidemiological evidence. *Int J Cancer*. 2009;125:171-180.
5. Lin H, An Y, Tang H, Wang Y. Alterations of bile acids and gut microbiota in obesity induced by high fat diet in rat model. *J Agric Food Chem*. 2019;67:3624-3632.
6. Natividad JM, Lamas B, Pham HP, et al. Bilophila wadsworthia aggravates high fat diet induced metabolic dysfunctions in mice. *Nat Commun*. 2018;9:2802.
7. Fu T, Coulter S, Yoshihara E, et al. FXR regulates intestinal cancer stem cell proliferation. *Cell*. 2019;176:1098-1112.e18.
8. Tong JL, Ran ZH, Shen J, Fan GQ, Xiao SD. Association between fecal bile acids and colorectal cancer: a meta-analysis of observational studies. *Yonsei Med J*. 2008;49:792-803.
9. Kühn T, Stepien M, López-Nogueroles M, et al. Prediagnostic plasma bile acid levels and colon cancer risk: a prospective study. *J Natl Cancer Inst*. 2020;112:516-524.
10. Dong W, Liu L, Dou Y, et al. Deoxycholic acid activates epidermal growth factor receptor and promotes intestinal carcinogenesis by ADAM17-dependent ligand release. *J Cell Mol Med*. 2018;22:4263-4273.
11. Liu L, Dong W, Wang S, et al. Deoxycholic acid disrupts the intestinal mucosal barrier and promotes intestinal tumorigenesis. *Food Funct*. 2018;9:5588-5597.
12. Cao H, Xu M, Dong W, et al. Secondary bile acid-induced dysbiosis promotes intestinal carcinogenesis. *Int J Cancer*. 2017;140:2545-2556.
13. Qiao K, Liu Y, Xu Z, et al. RNA m6A methylation promotes the formation of vasculogenic mimicry in hepatocellular carcinoma via Hippo pathway. *Angiogenesis*. 2021;24:83-96.
14. Zhao B, Wu M, Hu Z, et al. Thrombin is a therapeutic target for non-small-cell lung cancer to inhibit vasculogenic mimicry formation. *Signal Transduct Target Ther*. 2020;5:117.
15. Tachi M, Okada H, Matsuhashi N, et al. Human colorectal cancer infrastructure constructed by the glycocalyx. *J Clin Med*. 2019;8:1270.
16. Liu Z, Sun B, Qi L, Li H, Gao J, Leng X. Zinc finger E-box binding homeobox 1 promotes vasculogenic mimicry in colorectal cancer through induction of epithelial-to-mesenchymal transition. *Cancer Sci*. 2012;103:813-820.
17. Maniotis AJ, Folberg R, Hess A, et al. Vascular channel formation by human melanoma cells in vivo and in vitro: vasculogenic mimicry. *Am J Pathol*. 1999;155:739-752.
18. Wei X, Chen Y, Jiang X, et al. Mechanisms of vasculogenic mimicry in hypoxic tumor microenvironments. *Mol Cancer*. 2021;20:7.
19. Zeng Y, Yao X, Liu X, et al. Anti–angiogenesis triggers exosomes release from endothelial cells to promote tumor vasculogenesis. *J Extracell Vesicles*. 2019;8:1629865.
20. Treps L, Faure S, Clere N. Vasculogenic mimicry, a complex and devious process favoring tumorigenesis - interest in making it a therapeutic target. *Pharmacol Ther*. 2021;223:107805.
21. Zhang N, Zhang S, Wu W, et al. Regorafenib inhibits migration, invasion, and vasculogenic mimicry of hepatocellular carcinoma via targeting ID1-mediated EMT. *Mol Carcinog*. 2021;60:151-163.
22. Cao Z, Bao M, Miele L, Sarkar FH, Wang Z, Zhou Q. Tumour vasculogenic mimicry is associated with poor prognosis of human cancer patients: a systemic review and meta-analysis. *Eur J Cancer*. 2013;49:3914-3923.

23. Hernández de la Cruz ON, López-González JS, García-Vázquez R, et al. Regulation networks driving vasculogenic mimicry in solid tumors. *Front Oncol*. 2019;9:1419.

24. Kushi LH, Doyle C, McCullough M, et al. American Cancer Society Guidelines on nutrition and physical activity for cancer prevention: reducing the risk of cancer with healthy food choices and physical activity. *CA Cancer J Clin*. 2012;62:30-67.

25. Key TJ, Appleby PN, Bradbury KE, et al. Consumption of meat, fish, dairy products, and eggs and risk of ischemic heart disease. *Circulation*. 2019;139:2835-2845.

26. Wu Y, Du K, Guan W, et al. A novel definition of microvessel density in renal cell carcinoma: angiogenesis plus vasculogenic mimicry. *Oncol Lett*. 2020;20:192.

27. Liu T, Guo Z, Song X, et al. High-fat diet-induced dysbiosis mediates MCP-1/CCR2 axis-dependent M2 macrophage polarization and promotes intestinal adenoma-adenocarcinoma sequence. *J Cell Mol Med*. 2020;24:2648-2662.

28. Hagio M, Matsumoto M, Fukushima M, Hara H, Ishizuka S. Improved analysis of bile acids in tissues and intestinal contents of rats using LC/ESI-MS. *J Lipid Res*. 2009;50:173-180.

29. Yeo C, Han DS, Lee HJ, Lee EO. Epigallocatechin-3-gallate suppresses vasculogenic mimicry through inhibiting the Twist/VE-Cadherin/AKT pathway in human prostate cancer PC-3 cells. *Int J Mol Sci*. 2020;21:439.

30. Xiao T, Zhong W, Zhao J, et al. Polyphyllin I suppresses the formation of vasculogenic mimicry via Twist1/VE-cadherin pathway. *Cell Death Dis*. 2018;9:906.

31. Chen D, Jin D, Huang S, et al. Clostridium butyricum, a butyrate-producing probiotic, inhibits intestinal tumor development through modulating Wnt signaling and gut microbiota. *Cancer Lett*. 2020;469:456-467.

32. Wang C, Li P, Xuan J, et al. Cholesterol enhances colorectal cancer progression via ROS elevation and MAPK signaling pathway activation. *Cell Physiol Bioche*. 2017;42:729-742.

33. Park H, Kim M, Kwon GT, et al. A high-fat diet increases angiogenesis, solid tumor growth, and lung metastasis of CT26 colon cancer cells in obesity-resistant BALB/c mice. *Mol Carcinog*. 2012;51:869-880.

34. Xiu L, Yang Z, Zhao Y, et al. High-fat diets promote colon orthotopic transplantation tumor metastasis in BALB/c mice. *Oncol Lett*. 2019;17:1914-1920.

35. Yang J, Wei H, Zhou Y, et al. High-fat diet promotes colorectal tumorigenesis through modulating gut microbiota and metabolites. *Gastroenterology*. 2021;S0016-5085(21):03439–9.

36. Delgado-Bellido D, Serrano-Saenz S, Fernández-Cortés M, Oliver FJ. Vasculogenic mimicry signaling revisited: focus on non-vascular VE-cadherin. *Mol Cancer*. 2017;16:65.

37. Mercurio AM. VEGF/neuropilin signaling in cancer stem cells. *Int J Mol Sci*. 2019;20:490.

38. Lian L, Li XL, Xu MD, et al. VEGFR2 promotes tumorigenesis and metastasis in a pro–angiogenic-independent way in gastric cancer. *BMC Cancer*. 2019;19:183.

39. Chen J, Chen S, Zhuo L, Zhu Y, Zheng H. Regulation of cancer stem cell properties, angiogenesis, and vasculogenic mimicry by miR-450a-5p/SOX2 axis in colorectal cancer. *Cell Death Dis*. 2020;11:173.

40. Mitra D, Bhattacharyya S, Alam N, et al. Phosphorylation of EphA2 receptor and vasculogenic mimicry is an indicator of poor prognosis in invasive carcinoma of the breast. *Breast Cancer Res Treat*. 2020;179:359-370.

41. Zheng X, Huang F, Zhao A, et al. Bile acid is a significant host factor shaping the gut microbiome of diet-induced obese mice. *BMC Biol*. 2017;15:120.

42. Zhang W, Zhou P, Meng A, Zhang R, Zhou Y. Down-regulating Myoferlin inhibits the vasculogenic mimicry of melanoma via decreasing MMP-2 and inducing mesenchymal-to-epithelial transition. *J Cell Mol Med*. 2018;22:1743-1754.

43. Zhu Y, Liu X, Zhao P, Zhao H, Gao W, Wang L. Celastrol suppresses glioma vasculogenic mimicry formation and angiogenesis by blocking the PI3K/Akt/mTOR signaling pathway. *Front Pharmacol*. 2020;11:25.

44. Xie W, Zhao H, Wang F, et al. A novel humanized Frizzled-7-targeting antibody enhances antitumor effects of Bevacizumab against triple-negative breast cancer via blocking Wnt/β-catenin signaling pathway. *J Exp Clin Cancer Res*. 2021;40:30.

45. Zeng D, Zhou P, Jiang R, et al. Evodiamine inhibits vasculogenic mimicry in HCT116 cells by suppressing hypoxia-inducible factor 1-alpha-mediated angiogenesis. *Anticancer Drugs*. 2021;32:314-322.

46. Zong S, Tang Y, Li W, et al. A Chinese herbal formula suppresses colorectal cancer migration and vasculogenic mimicry through ROS/HIF-1α/MMP2 pathway in hypoxic microenvironment. *Front Pharmacol*. 2020;11:705.

47. Eelen G, Treps L, Li X, Carmeliet P. Basic and therapeutic aspects of angiogenesis updated. *Circ Res*. 2020;127:310-329.

48. Zheng N, Zhang S, Wu W, Zhang N, Wang J. Regulatory mechanisms and therapeutic targeting of vasculogenic mimicry in hepatocellular carcinoma. *Pharmacol Res*. 2021;166:105507.

49. Liu JJ, Tang W, Fu M, et al. Development of R(8) modified epirubicin-dihydroartemisinin liposomes for treatment of non-small-cell lung cancer. *Artif Cells Nanomed Biotechnol*. 2019;47:1947-1960.

50. Luo Q, Wang J, Zhao W, et al. Vasculogenic mimicry in carcinogenesis and clinical applications. *J Hematol Oncol*. 2020;13:19.

51. Yang J, Antin P, Berx G, et al. Guidelines and definitions for research on epithelial-mesenchymal transition. *Nat Rev Mol Cell Biol*. 2020;21:341-352.

52. Qi L, Sun B, Liu Z, Cheng R, Li Y, Zhao X. Wnt3a expression is associated with epithelial-mesenchymal transition and promotes colon cancer progression. *J Exp Clin Cancer Res*. 2014;33:107.

53. Ribatti D, Tamma R, Annese T. Epithelial-mesenchymal transition in cancer: a historical overview. *Transl Oncol*. 2020;13:100773.

54. Singh M, Yelle N, Venugopal C, Singh SKEMT. Mechanisms and therapeutic implications. *Pharmacol Ther*. 2018;182:80-94.

55. Li W, Zong S, Shi Q, Li H, Xu J, Hou F. Hypoxia-induced vasculogenic mimicry formation in human colorectal cancer cells: involvement of HIF-1a, Claudin-4, and E-cadherin and vimentin. *Sci Rep*. 2016;6:37534.

56. Burnat G, Rau T, Elshimi E, Hahn EG, Konturek PC. Bile acids induce overexpression of homeobox gene CDX-2 and vascular endothelial growth factor (VEGF) in human Barrett's esophageal mucosa and adenocarcinoma cell line. *Scand J Gastroenterol*. 2007;42:1460-1465.

57. Chen L, Lin G, Chen K, et al. VEGF promotes migration and invasion by regulating EMT and MMPs in nasopharyngeal carcinoma. *J Cancer*. 2020;11:7291-7301.

58. Sadremomtaz A, Kobarfard F, Mansouri K, Mirzanejad L, Asghari SM. Suppression of migratory and metastatic pathways via blocking VEGFR1 and VEGFR2. *J Recept Signal Transduct Res*. 2018;38:432-441.

59. Hultgren NW, Fang JS, Ziegler ME, et al. Slug regulates the Dll4-Notch-VEGFR2 axis to control endothelial cell activation and angiogenesis. *Nat Commun*. 2020;11:5400.

60. Prado M, Macedo S, Guiraldelli GG, et al. Investigation of the prognostic significance of vasculogenic mimicry and its inhibition by sorafenib in canine mammary gland tumors. *Front Oncol*. 2019;9:1445.

61. Witte HM, Riecke A, Steinestel K, et al. The addition of chloroquine and bevacizumab to standard radiochemotherapy for recurrent glioblastoma multiforme. *Br J Neurosurg*. 2021;1-13.

62. Xu Y, Li Q, Li XY, Yang QY, Xu WW, Liu GL. Short-term anti–vascular endothelial growth factor treatment elicits vasculogenic mimicry formation of tumors to accelerate metastasis. *J Exp Clin Cancer Res*. 2012;31:16.

63. Ocvirk S, Wilson AS, Posma JM, et al. A prospective cohort analysis of gut microbial co-metabolism in Alaska Native and rural African people at high and low risk of colorectal cancer. *Am J Clin Nutr*. 2020;111:406-419.

64. Hugenholtz F, de Vos WM. Mouse models for human intestinal microbiota research: a critical evaluation. *Cell Mol Life Sci*. 2018;75:149-160.